



**HAL**  
open science

## Controlling the MC and M<sub>2</sub>C carbide precipitation in Ferrium® M54® steel to achieve optimum ultimate tensile strength/fracture toughness balance

Aurélien Mondière, Valentine Déneux, Nicolas Binot, Denis Delagnes

### ► To cite this version:

Aurélien Mondière, Valentine Déneux, Nicolas Binot, Denis Delagnes. Controlling the MC and M<sub>2</sub>C carbide precipitation in Ferrium® M54® steel to achieve optimum ultimate tensile strength/fracture toughness balance. *Materials Characterization*, 2018, 140, p.103 - 112. 10.1016/j.matchar.2018.03.041 . hal-01761384

**HAL Id: hal-01761384**

**<https://imt-mines-albi.hal.science/hal-01761384>**

Submitted on 11 Apr 2018

**HAL** is a multi-disciplinary open access archive for the deposit and dissemination of scientific research documents, whether they are published or not. The documents may come from teaching and research institutions in France or abroad, or from public or private research centers.

L'archive ouverte pluridisciplinaire **HAL**, est destinée au dépôt et à la diffusion de documents scientifiques de niveau recherche, publiés ou non, émanant des établissements d'enseignement et de recherche français ou étrangers, des laboratoires publics ou privés.

# Controlling the MC and M<sub>2</sub>C carbide precipitation in Ferrium® M54® steel to achieve optimum ultimate tensile strength/fracture toughness balance

A. Mondiere<sup>a,\*</sup>, V. Déneux<sup>b</sup>, N. Binot<sup>b</sup>, D. Delagnes<sup>a</sup>

<sup>a</sup> Université de Toulouse, CNRS, Mines Albi, INSA, UPS, ISAE-SUPAERO, ICA (Institut Clément Ader), Campus Jarlard, F-81013 Albi, France

<sup>b</sup> Safran Landing Systems, F-64400 Bidos, France

## Keywords:

UHS steel

Undissolved carbides

M<sub>2</sub>C secondary carbides

Dilatometry

Thermodynamic calculations

Atom probe tomography

## ABSTRACT

Ferrium® M54® exhibits an excellent UTS/K<sub>1C</sub> balance allowing its application in aeronautical structures. This steel belongs to the Co-Ni UHS steels family with M<sub>2</sub>C nanometer-size carbide precipitation during tempering. These steels provide very high strength with a very good fracture toughness thanks to the M<sub>2</sub>C fine precipitation during tempering, but also because coarse particles are dissolved during austenitizing without grain coarsening. The goal of this article is to identify the different carbide populations in M54®. A small addition of Ti in M54® forms a Ti-rich MC carbide precipitation that is stable at high temperature. Consequently, during austenitization at 1060 °C, all other types of coarse carbides are dissolved in the matrix without grain coarsening. As a very small part of the initial carbon content is needed to form MC carbides, efficient and intensive nanometric M<sub>2</sub>C carbide precipitation takes place during tempering, leading to very high final strength. Due to this double precipitation of carbides in M54®, the steel achieves an outstanding UTS/K<sub>1C</sub> balance.

## 1. Introduction

Aircraft applications, particularly for landing gear, require steels with high mechanical resistance, fracture toughness and stress corrosion cracking resistance [1]. Additionally, the aerospace industry is looking for different ways to reduce the weight of landing gear parts, as the landing gear assembly can represent up to 7% of the total weight of the aircraft [2]. The search for metal alloys with a better balance of mechanical properties while maintaining a constant production cost is stimulating research activities. For several decades, 300 M steel has been widely used for landing gear applications. However, its fracture toughness and stress corrosion cracking resistance need to be improved and aeronautical equipment suppliers are searching for new grades. As shown in Fig. 1, AerMet® 100 and Ferrium® M54® (M54®) grades are excellent candidates to replace the 300 M steels without any reduction in strength or increase in weight. Other grades do not present a high enough fracture toughness, or are not resistant enough.

The recent development of M54® steel since 2010 [4] has led to a higher stress corrosion cracking resistance and lower cost due to its lower cobalt content (see Table 1), as compared to the equivalent properties of the AerMet® 100 grade. These two steels belong to the UHS Co-Ni steel family.

UHS Co-Ni steels were developed at the end of 1960s with the HP9-4-X [5] and HY-180 [6] grades, with the main goal being to achieve

higher fracture toughness than 300M or 4340 steels. The main idea was first to replace cementite by M<sub>2</sub>C alloy carbide precipitation during tempering to avoid brittle fracture without too large reduction in mechanical strength. A better balance of UTS/K<sub>1C</sub> was achieved with AF1410 [7] by increasing the content of carbide-forming elements. In addition, an improvement in fracture toughness was also requested and finally achieved by the accurate control of reverted austenite precipitation during tempering [8] and the addition of rare earth elements to change the sulfide type [9,10], resulting in an increase in inclusion spacing [11]. Thus, AerMet® 100 was patented in 1993 [12], incorporating these scientific progress to achieve the same strength level of 300 M but with a higher fracture toughness. Then, from the 1990s to the 2000s, scientists sought to improve the grain boundary cohesion to further increase the fracture toughness by W, Re and B additions [13]. Thus, Ferrium® S53® steel, developed in 2007 [14], was the first steel of the family containing W. Seven years ago, Ferrium® M54® steel was designed, offering a steel with roughly the same mechanical properties as AerMet® 100, but with a lower price thanks to a lower cobalt content.

UHS Co-Ni steels all exhibit an excellent UTS/K<sub>1C</sub> balance due to a M<sub>2</sub>C carbide precipitation during tempering in a highly dislocated lath-martensitic matrix [4,7,12,15–17]. However, there is limited literature on the recently developed M54® steel [18–21].

The addition of alloying elements in UHS Co-Ni steels also forms stable carbides like M<sub>6</sub>C or M<sub>23</sub>C<sub>6</sub> during the heat treatment process.

\* Corresponding author.

E-mail address: aurelien.mondiere@mines-albi.fr (A. Mondiere).

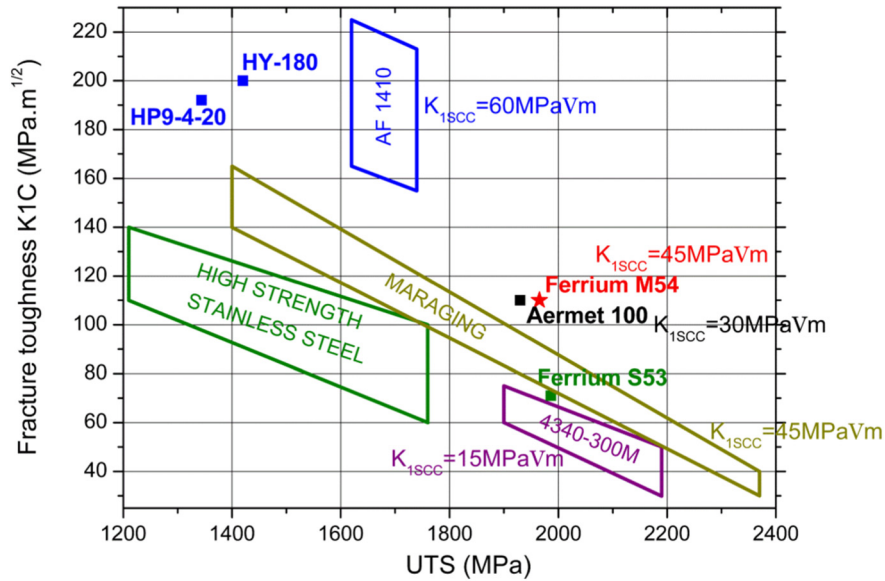


Fig. 1. Comparison of different grades of steel according to their fracture toughness, ultimate tensile strength and stress corrosion cracking resistance (adapted from [3]).

Table 1  
Chemical composition (wt%) of UHS Co-Ni steels.

	C	Cr	Ni	Co	Mo	W	V	Ti	Mn	Si
M54*	0.3	1	10	7	2	1.3	0.1	0.02max	/	/
Aermet* 100	0.23	3.1	11.1	13.4	1.2	/	/	0.05max	/	/
AF1410	0.15	2	10	14	1	/	/	0.015	0.1	0.1
HP9-4-20	0.2	0.8	9	4	1	/	0.08	/	0.2	0.2
HY-180	0.13	2	10	8	1	/	/	/	0.1	0.05
S53*	0.21	10	5.5	14	2	1	0.3	0.2max	/	/

The size of these stable carbides can easily reach several 100 nm, resulting in a significant decrease in fracture toughness by acting as microvoid nucleation sites during the mechanical load [22]. These particles can be dissolved by increasing the austenitizing temperature, but the prior austenite grain size rapidly increases and induces a detrimental effect on the mechanical properties [23]. The new challenge for these steels is thus to dissolve coarse stable carbides without an excessive grain growth.

This challenge is also well-known in other kinds of martensitic steels for other applications, such as hot work tool steels. Michaud [24] showed that V-rich carbide precipitation during tempering achieves high mechanical properties at room temperature as well as at high temperature. However, precipitation stayed heterogeneously distributed in the matrix, regardless of the austenitizing and tempering conditions, and so fracture toughness and Charpy impact were limited. Indeed, the same V-rich precipitation (MC type) that controls the austenitic grain size during austenitizing and controls the strength during tempering were identified. The incomplete solutionizing of V-rich carbides during austenitizing does not permit a homogeneous concentration of alloying elements in the martensitic matrix after quench, which explains why the strength/fracture toughness balance is limited. The generic idea would be to introduce a double/different precipitation with a single and precise role for each population: to control the austenitic grain size OR to control the mechanical strength. In H11-type tool steels, the addition of Mo slightly improved the balance of properties [24].

In steels for aircraft applications, Olson [25] and Gore et al. [26] succeeded in introducing another type of homogeneous small particles which pin the grain even for elevated austenitization temperatures

( $T = 1200^\circ\text{C}$ ) in AF1410: (Ti,Mo)(C,N). These carbides avoid grain coarsening between  $815^\circ\text{C}$  and  $885^\circ\text{C}$  at austenitization leading to an increase in fracture toughness due to coarse carbides dissolution [22]. The patent of Ferrium® S53® steel also describes a nanoscale MC precipitation which pins the grain boundary and avoids grain coarsening by the dissolution of the coarse carbides [14].

Stable carbide dissolution in Ferrium® M54® seems to be particularly challenging due to the formation of both  $M_2C$  and  $M_6C$  Mo-rich carbides during the heat treatment process (see Fig. 2). Indeed, as Mo-rich  $M_2C$  carbides precipitate during tempering, the full dissolution of Mo-rich carbides is needed to achieve a homogeneous distribution of Mo within the matrix.

More specifically, particles that control the austenitic grain size need to be stable enough at high temperature to dissolve the whole population of  $M_2C$  and  $M_6C$  carbides without grain coarsening. The aim of this article is to investigate carbides precipitation in M54® after a cryogenic treatment following the quench as well as after tempering. Carbide distribution, size and composition are carefully described for both states.

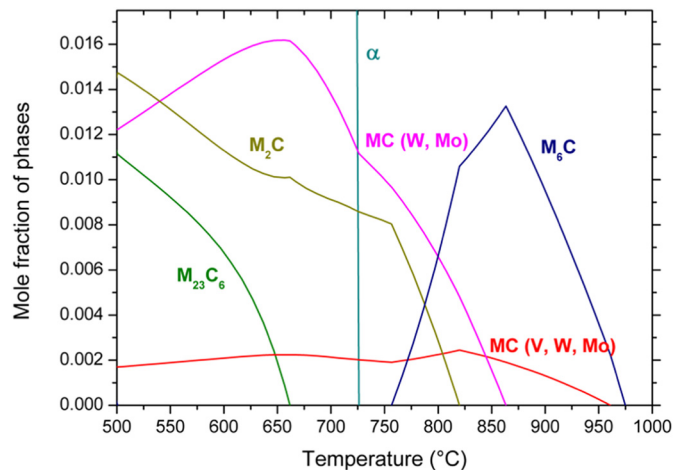


Fig. 2. Mole fraction of phase according to austenitizing temperature in M54® calculated with TCFE3 ThermoCalc® database (Ti-free).

## 2. Experiments

### 2.1. Materials and Heat Treatment

Specimens were taken at mid-radius of a single bar of diameter 10.25 cm in the longitudinal direction.

The performed heat treatments were in agreement with the QuesTek recommendations [27] and consisted of a preheating treatment at 315 °C/1 h, a solutionizing at 1060 °C/1 h, followed by an oil quench, cold treatment at −76 °C/2 h and tempering at 516 °C/10 h.

### 2.2. Experimental Techniques

Austenite grain size was measured after the quench. Precipitation in the quenched state, after cryogenic treatment, was observed to identify undissolved carbides. Secondary carbides were characterized after tempering, at the end of the whole heat treatment process.

Chemical composition of the alloy was measured with a Q4 Tasman Spark Optical Emission Spectrometer from Bruker.

Dilatometry was performed using a Netzsch apparatus, DIL402C. Samples for dilatometry were in the form of a cylinder of diameter 3,7 mm with a length of 25 mm. Samples were heated at 7 °C/min and cooled at 5 °C/min under argon atmosphere.

For the as-quenched state, carbides were extracted by chemical dissolution of the matrix with a modified Berzelius solution at room temperature [28] as already developed by Cabrol et al. [29]. At the end of the dissolution, the solution was centrifuged to collect nanoscale precipitates. A Beckman Coulter Avanti J-30I centrifugal machine equipped with a JA-30.50Ti rotor was used to centrifuge the solution. The experimental method is described precisely in [29].

XRD characterizations of the powder obtained after the chemical dissolution and of the bulk sample were performed using a Panalytical X'Pert PRO diffractometer equipped respectively with a Cu or Co radiation source. Phase identification was achieved by comparing the diffraction pattern of the experimental samples with reference JCPDS patterns.

Prior austenite grain size measurement is difficult because of the very low impurity content in the grade M54®. An oxidation etching was conducted by heating polished samples in a furnace at a temperature of 900 °C and 1100 °C under room atmosphere for 1 h and slightly polishing them after quenching to remove the oxide layer inside the grains and keeping the oxide only at the grain boundary.

Transmission Electron Microscopy (TEM) observations were performed using a JEOL JEM 2100F. Thin foils for TEM were cut from the specimens and the thickness was reduced to approximately 150 µm. Then, they were cut into disks and polished to a thickness of about 60 µm. The thin foils were then electropolished in a perchloric acid-methanol solution at −15 °C with a TenuPol device.

Chemical composition at nanometer scale was determined using atom probe tomography (APT) at the Northwestern University Center for Atom-Probe Tomography (NUCAPT). Samples were prepared into rods with a cross section of 1 x 1 mm<sup>2</sup> and electro-polished using a two-step process at room temperature [30,31]. The APT analyses were conducted with a LEAP 4000X-Si from Cameca at a base temperature of −220 °C, a pulse energy of 30 pJ, a pulse repetition rate of 250 kHz, and an ion detection rate of 0.3% to 2%. This instrument uses a local-electrode and laser pulsing with a picosecond 355 nm wavelength ultraviolet laser, which minimizes specimen fracture [32].

For the prediction of the different types and molar fraction of each phase according to temperatures, thermodynamics calculations were performed using ThermoCalc® software. This software and database were developed at the Royal Institute of Technology (KTH) in

Stockholm [33]. ThermoCalc® calculations were performed using the TCFe3 database.

## 3. Results and Discussions

### 3.1. Discussion of Optimized Mechanical Properties With Finely Dispersed Nanometer Size Precipitation

Research activities on UHS steels for aircraft applications focus on maximizing mechanical strength without decreasing the fracture toughness and stress corrosion cracking resistance. To improve strength, dislocations mobility must be reduced. Consequently, increasing the number density of secondary particles (N<sub>p</sub>) is a well-known method and the resulting hardening is given by the following equation [23]:

$$\Delta\sigma_p \approx \frac{Gb(f)^{0.5}}{d} \quad (1)$$

where  $\Delta\sigma_p$  is particle contribution to the yield strength, G is the shear modulus, d is the particle diameter, f the volume fraction of the particle and b the Burgers vector of dislocations.

Indeed, for the same volume fraction, a small particles distribution leads to a better yield strength, due to the decrease in dislocation mobility.

To obtain this fine and dispersed precipitation, two different types of nucleation are generally observed to occur in UHS steels:

- Numerous preferential nucleation sites leading to heterogeneous nucleation;
- Homogeneous supersaturation of carbide-forming elements.

For the first condition, the heterogeneous nucleation of M<sub>2</sub>C carbides on dislocations has already been observed in previous works [34,35]. Indeed, dislocation sites are energetically favorable due to atom segregation and the short diffusion path offered to the diffusing element (pipe diffusion). It is therefore important to maintain a high dislocation density during tempering. Consequently, cobalt is added to these alloys to keep a high dislocation density during tempering. As previously described in the literature [13,25], Co delays the dislocation recovery through the creation of short-range ordering (SRO) in the matrix. Co also decreases the solubility of Mo in ferrite and increases the carbon activity inside ferrite [34,36–39], leading to a more intensive precipitation of M<sub>2</sub>C carbides.

The main criterion for accessing the second condition is related to the dissolution carbides during austenitizing. If carbides are not totally solutionized, the precipitation during tempering will be heterogeneously dispersed with a higher density of clusters in the areas of high concentration of the carbide-forming elements. To avoid heterogeneous concentration, remaining carbides from the previous stage of heat treatment should be totally dissolved and enough time should be spent at a temperature above the carbide solvus to obtain a homogeneous composition of the carbide-forming elements in austenite. Moreover, in order to obtain a fine and dispersed precipitation during tempering, the driving force must be increased by increasing the supersaturation resulting in a higher nucleation rate [35]. Furthermore, undissolved carbides also reduce the potential volume fraction of particles that may precipitate during tempering [40] and almost total dissolution is needed. Thus, the austenitizing condition should be rationalized based on the carbide dissolution kinetics and diffusion coefficient of alloying elements in the matrix to obtain a homogeneous chemical composition of the carbide-forming elements in the martensitic matrix in the as-quenched state.

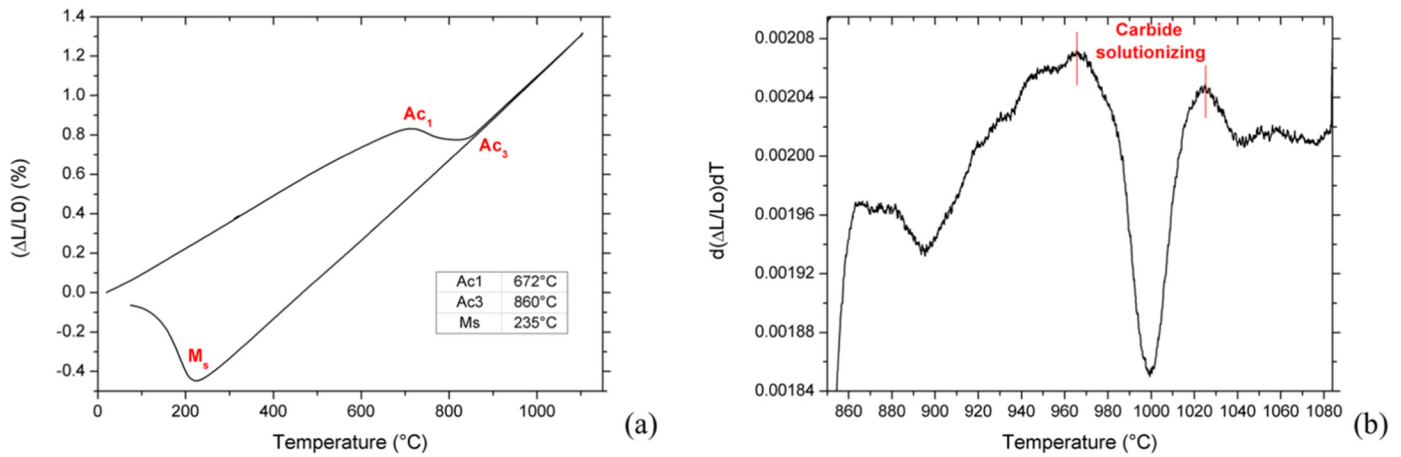


Fig. 3. Relative length change curve (a) and derivative of the relative change curves (b) obtained from dilatometer heating experiments.

### 3.2. Identification of Carbide Solutionizing Temperature

The temperatures of phase transformation were determined by dilatometry experiments. According to the relative length change shown in Fig. 3(a),  $Ac_1$ ,  $Ac_3$  and  $M_s$  temperatures are clearly detected. To detect the solutionizing of carbides, the derivative of the relative length change was calculated. Carbide dissolution takes place at a temperature ranging from 970 °C to 1020 °C, as shown in Fig. 3(b).

If the austenitizing temperature is not high enough, undissolved carbides are clearly observed (see Fig. 4) and slightly decrease UTS from 1997 MPa at 1060 °C to 1982 MPa at 1020 °C, which is probably due to the carbon trapped inside those undissolved particles.

These coarse carbides can also be observed after polishing and a Nital 2% etch using SEM (Fig. 5). The volume fraction seems to be

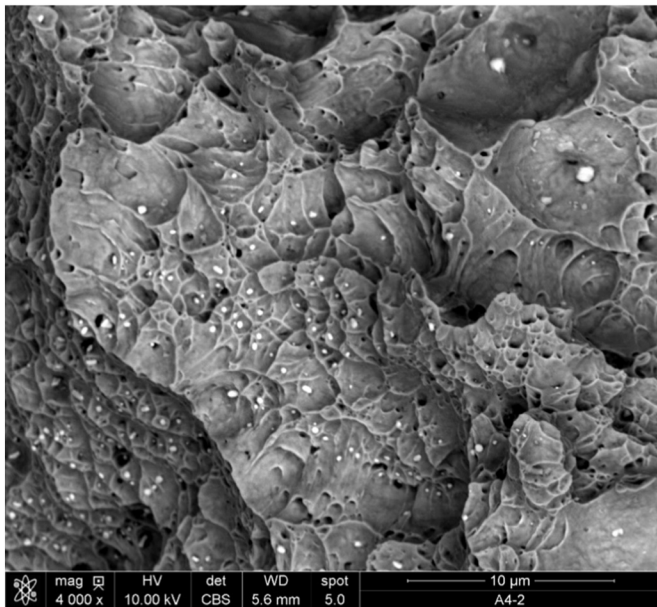


Fig. 4. SEM image of a fracture surface of a tensile specimen (austenitization performed at 1020 °C).

particularly high.

According to ThermoCalc® calculations, these undissolved carbides obtained after 1 h at 1020 °C are  $M_6C$  carbides (see Fig. 2) containing a significant amount of W (see Table 2).

The high solutionizing temperature of the M54® steel as compared to other steels of the same family (free of W, see Table 3) is due to the tungsten addition which stabilizes the  $M_6C$  carbides. If the austenitizing temperature is not high enough, undissolved carbides still remain (see Fig. 4 and Fig. 5) and the tensile properties (yield strength, UTS, elongation at rupture), as well as fatigue resistance are reduced. However, if the austenitizing temperature is too high and no carbides remain, a huge grain size coarsening can be observed also leading to a decrease in the usual mechanical properties.

According to Naylor and Blondeau [41], thinner laths and lath packets, directly dependent on austenite grain size [23], can improve fracture toughness by giving a long and winding route to the crack during rupture. Białobrzaska et al. [42] have clearly shown that at room temperature, strength, yield strength, fatigue resistance and impact energy increase when the average austenite grain size decreases. Thus, any coarsening of austenite grains should be avoided.

### 3.3. Pinning of the Grain Boundary and Chemical Homogenization of the Austenitic Matrix at 1060 °C

As previously mentioned in the introduction, to control the grain size during austenitizing without any impact on precipitation during tempering, the precipitation of two types of particles is needed: one type to control the grain size during solutionizing and the second type of particles which precipitates during tempering.

To achieve this goal, one way is to add MC type precipitation to avoid quick coarsening of austenitic grains. However, according to ThermoCalc® calculations, the MC solvus temperature is not sufficiently high to allow the total dissolution of  $M_6C$  carbides (see Fig. 2). Thus, Olson [25] and Gore [26] added some Ti to form more stable MC carbides and dissolve other coarse stable carbides. A little addition of Titanium is sufficient to obtain a significant effect on the grain size, as described by Kantner who adds 0.04%mass [13] of titanium in Fe-

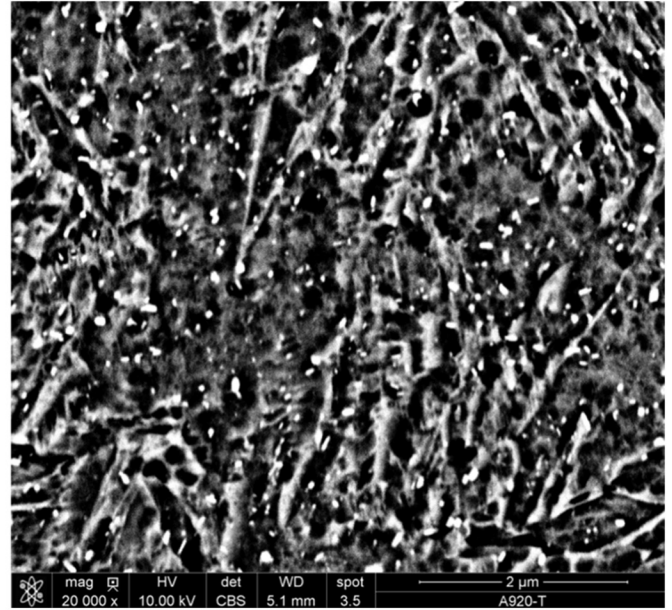
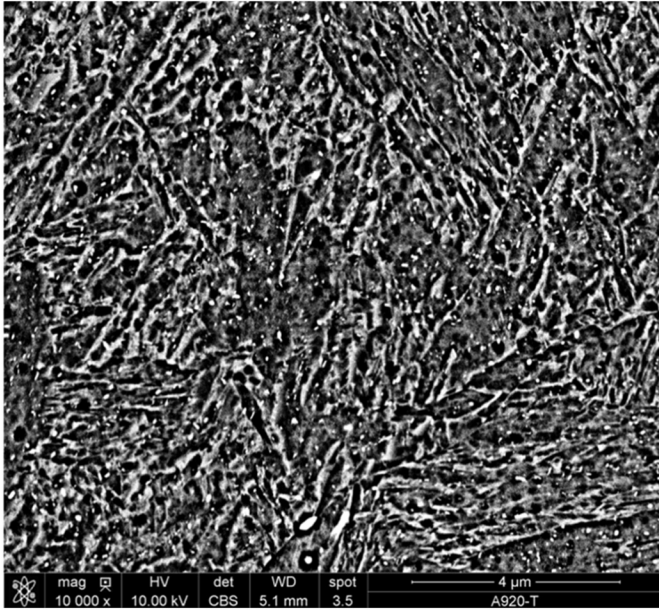


Fig. 5. SEM image of an as-quenched sample austenitized at 920 °C after nital etch.

**Table 2**  
Composition of  $M_6C$  carbides predicted by ThermoCalc® calculations.

Carbide	$M_6C$
Composition (860 °C)	(Fe <sub>2.8</sub> Mo <sub>2.05</sub> W <sub>0.96</sub> Cr <sub>0.12</sub> V <sub>0.07</sub> )C

**Table 3**  
Austenitization of different UHS steels hardened by  $M_2C$  carbide precipitation.

Steel	M54®	AerMet® 100	AF1410
$T_{aust}$ (°C)	1060	885	843

15Co-6Ni-3Cr-1.7Mo-2 W-0.25C and Fe-15Co-5Ni-3Cr-2.7Re-1.2 W-0.18C steels, or Lippard who adds only 0.01%mass [43] in alloys AF1410, AerMet® 100, MTL2 and MTL3. A low volume fraction of thin particles seems to be efficient in preventing austenitic grain growth [26]. Indeed, an addition of 0.01%mass of Ti in the M54® grade is enough to shift the MC solvus temperature by approximately 100 °C above the MC solvus temperature of the M54® grade free of Titanium according to ThermoCalc® calculation (see Fig. 6).

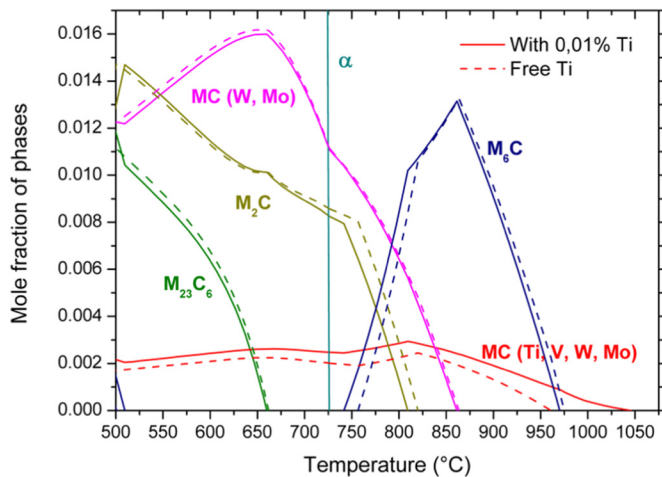


Fig. 6. Mole fraction of phase according to austenitizing temperature in M54® with and without 0.01%mass Ti calculated with TCFE3 ThermoCalc® database.

Moreover, MC carbides contain a large amount of Ti (see Fig. 7) which is not the case for  $M_2C$  precipitation during tempering. Consequently, Ti-rich MC carbides seem relevant, to be a solution to control the grain size without any impact on precipitation during tempering. The purpose of the following paragraph is to compare the experimental results with the above-mentioned theoretical prediction.

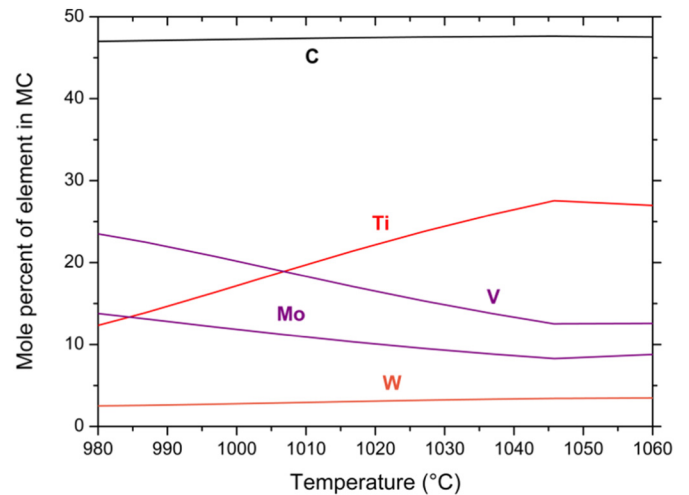


Fig. 7. Composition of MC carbide according to the temperature calculated with TCFE3 ThermoCalc® database.

After austenitizing for 1 h at 1060 °C, fine undissolved carbides were found in the as-quenched state after cryogenic treatment in M54® steels. These carbides are thinner than the undissolved carbides observed. In addition, a lower volume fraction is measured after an austenitization at 1060 °C than after a 1020 °C or 920 °C austenitization (see Fig. 8). The average size of these carbides is around 70 nm, measured on a sample of 23 carbides sample. In addition, no coarse undissolved carbides are observed indicating that the optimal austenitization conditions are not far to be reached.

Chemical extraction of carbides in the as-quenched state was performed to determine the type of those undissolved carbides still remaining after a 1060 °C austenitizing. As predicted by the thermocalc calculation, a FCC structure (type MC) was clearly identified from the

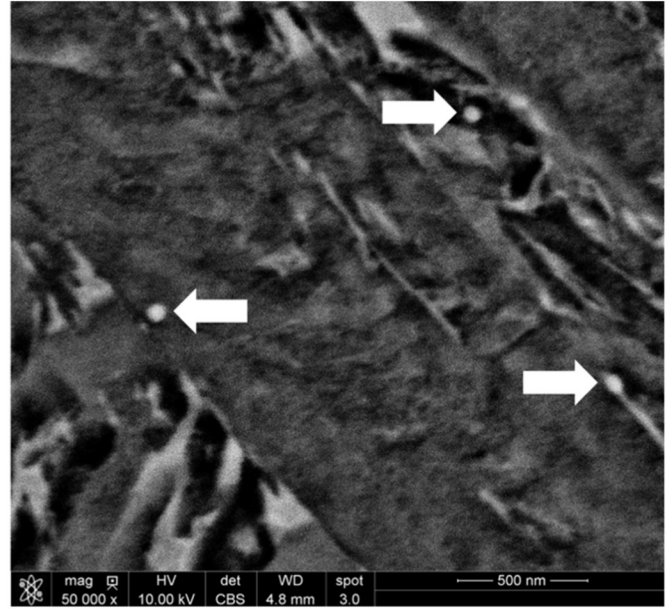
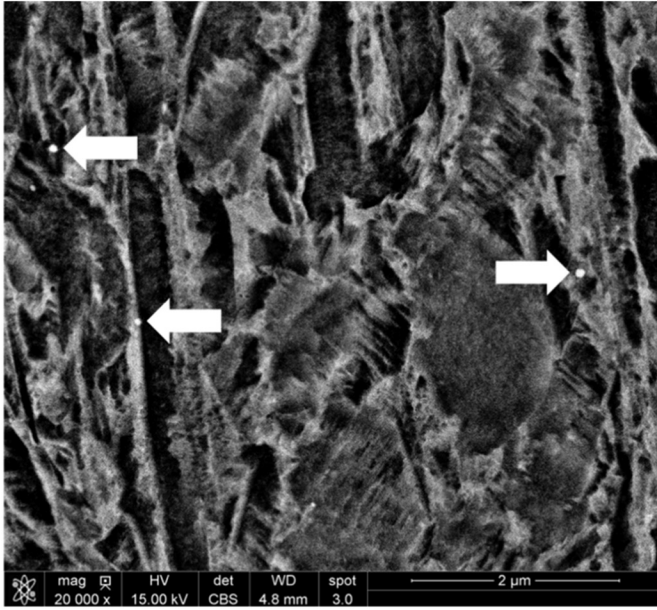


Fig. 8. SEM observations of undissolved carbides after 1060 °C austenitizing and Nital etch (as-quenched structure).

XRD patterns (see Fig. 9). Moreover, the chemical composition measured by EDX (Energy Dispersive X-ray spectroscopy) is  $(\text{Ti}_{0.44}\text{Mo}_{0.27}\text{W}_{0.13}\text{V}_{0.16})\text{C}$ . This composition is in quite good agreement with the ThermoCalc® calculated composition  $(\text{Ti}_{0.55}\text{V}_{0.25}\text{Mo}_{0.17}\text{W}_{0.08})\text{C}_{0.95}$ .

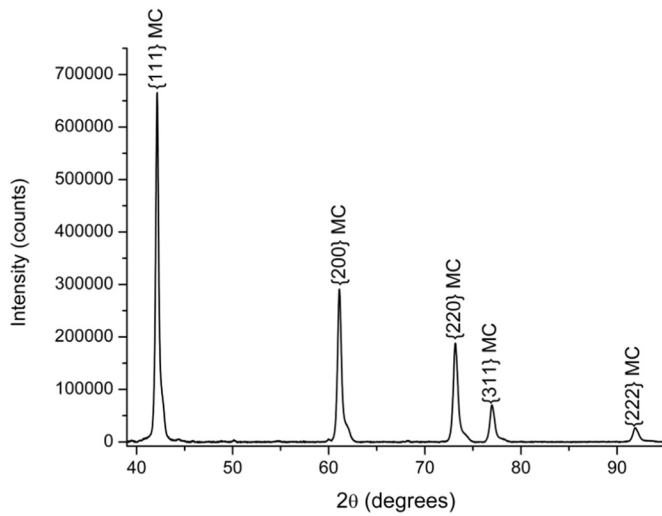


Fig. 9. Pattern and experimental XRD profiles (relative intensities) of precipitates extracted from the as-quenched M54® steel.

According to Spark Optical Emission Spectrometer measurements, the average Ti concentration measured is about 0.013 wt% in M54® steel. Considering that all the Ti atoms precipitate and taking into account the chemical composition of the MC measured by EDX, the volume fraction of Ti-rich MC carbide is found to be nearly 0.06%.

The intercarbide distance can be estimated using the equation given by Daigne et al. [44]:

$$d = 1.18 \times r_{\text{particle}} \sqrt{\frac{2\pi}{3f_v}} \quad (2)$$

where  $d$  is the distance between particles,  $r$  is the radius of the particle and  $f_v$  the volume fraction of particles.

According to Eq. (2), the distance between the MC carbides with an addition of 0.013 wt% of Ti is about a micrometer. This value is in very good agreement with SEM observations (see Fig. 8) indicating that most of the titanium carbides remain undissolved after the austenitization at 1060 °C.

Furthermore, a relation has been developed in tool steels to describe the grain refinement by a particle dispersion in tool steels. Bate [45] suggested the following equation between the limiting grain size diameter  $D$ , the mean radius,  $r$ , and the volume fraction  $F_v$  of the pinning particles:

$$D = \frac{4r}{3F_v} \quad (3)$$

The calculated average grain size diameter is 78 μm according to the Bate's Eq. (3) in M54®.

This value is in a very good agreement with the measured average grain size of  $81 \pm 39 \mu\text{m}$  at 900 °C or  $79 \pm 38 \mu\text{m}$  at 1100 °C (see Fig. 10). Approximately 300 grains were measured for each austenitizing temperature. According to the Bate's work, the estimated 0.06% volume fraction of undissolved MC carbides is sufficient to control the grain size of austenite.

Consequently, MC particles need only a very small quantity of carbide-forming elements required for  $\text{M}_2\text{C}$  precipitation during tempering. In addition, the calculated diffusion lengths of the different carbide-forming elements, Mo, Cr, W, are clearly significantly higher than the distance between first neighbors of Mo, Cr, W, respectively in

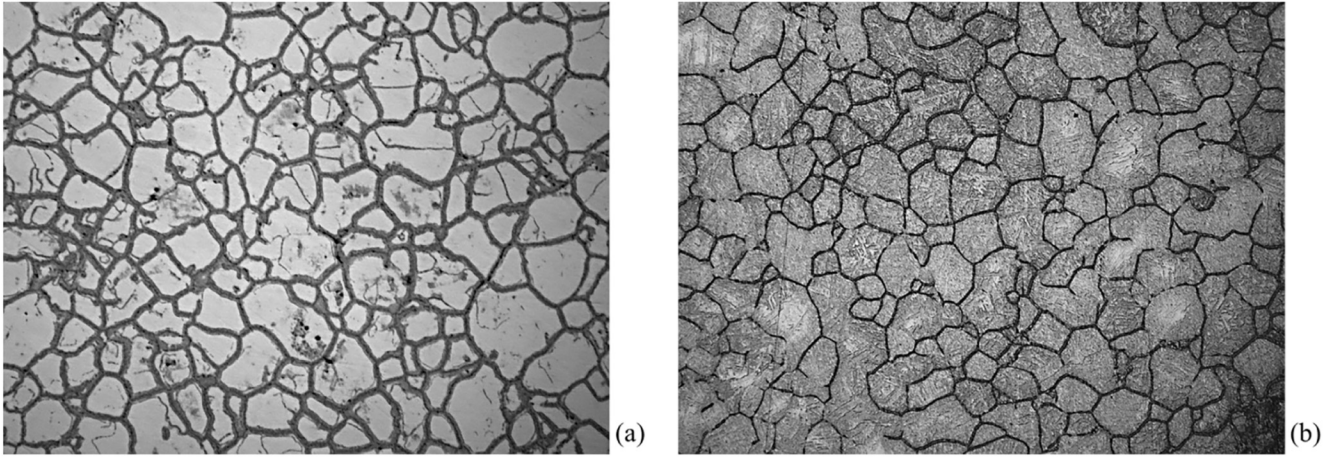


Fig. 10. Prior austenitic grain size in as-quenched state after 1 h austenitizing at 900 °C (a) and 1100 °C (b).

Table 4

Diffusivity in  $\gamma$ -iron and diffusion distance during solutionizing of carbide-forming elements.

Element	Mo	Cr	W
Diffusivity in $\gamma$ -iron (D, cm <sup>2</sup> /s)	0.036exp (-239,8/RT) [46]	0.063exp (-252,3/RT) [46]	0.13exp (-267,4/RT) [46]
Diffusion distance during austenitization (1 h at 1060 °C) ( $\mu$ m)	~4	~3	~2

### 3.4. Precipitation During Tempering

The particles that precipitate during tempering are totally different from the carbides controlling the austenitic grain size. According to XRD results,  $M_2C$ -type carbides are identified after a tempering for 500 h at 516 °C (see Fig. 11). This long duration of tempering is necessary to detect the diffraction peaks of  $M_2C$  carbides. For the standard tempering of 10 h, the volume fraction and the size of carbides might be too low to be detected by XRD, or long-distance ordering of  $M_2C$  carbides (hexagonal structure) might not be achieved as already suggested by Machmeier et al. [47].

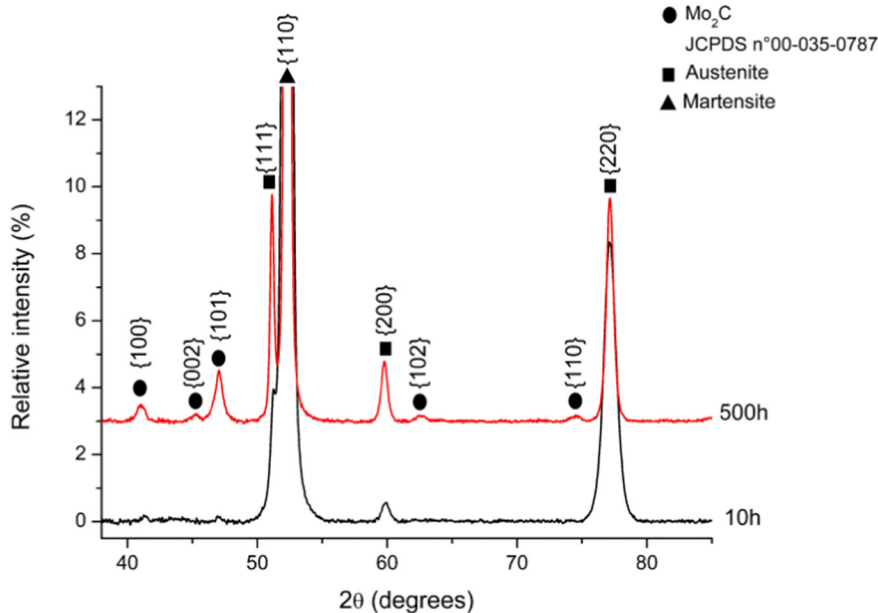


Fig. 11. Reference JCPDS pattern and experimental XRD profiles (relative intensities) of samples tempered at 516 °C for 10 h and 500 h.

the austenitic matrix at the end of austenitization (1060 °C/1 h) (see Table 4). As a consequence, homogeneous composition of the austenite is quickly obtained before quenching.

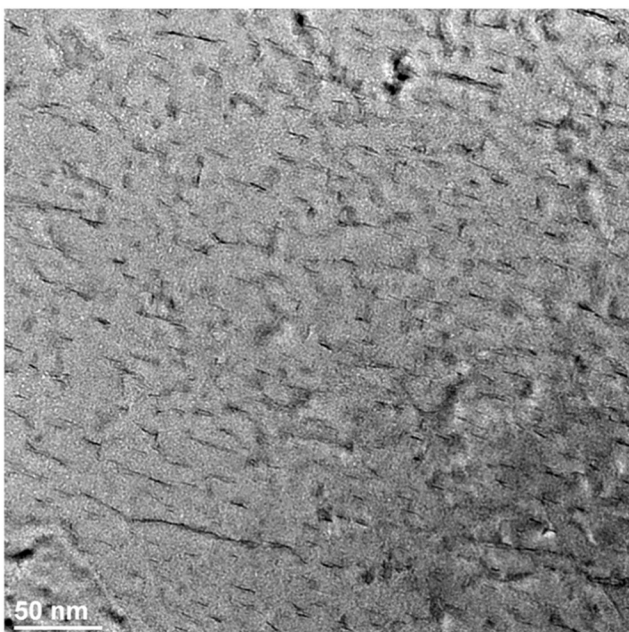
By way of conclusion, a small amount of Ti-rich MC carbides control the austenitic grain size and above all, the complete dissolution of  $M_6C$  molybdenum rich carbides leads to the homogeneous distribution of the  $M_2C$  carbide-forming elements before quenching.

Consequently, the same carbide type is identified in the M54<sup>®</sup>, AerMet<sup>®</sup> 100 and AF1410 steels [15,48]. Atom probe analyses were performed to determine the distribution of  $M_2C$  carbides within the martensitic matrix and to estimate the chemical composition of  $M_2C$  carbides. To define the particle/matrix interface found in the analyzed box, the adopted criterion is an isoconcentration of 36 at% of Molybdenum + Carbon. Carbides seem to be homogeneously distributed within the matrix according to the (limited) volume analyzed by APT (see Fig. 12).



**Fig. 12.** Three-dimensional APT reconstruction of Ni atoms (green) of a sample tempered at 516 °C for 10 h. Carbides are represented as violet isoconcentration surfaces (total concentration of Mo and C is 36 at. pct). (For interpretation of the references to color in this figure legend, the reader is referred to the web version of this article.)

According to TEM observations, the precipitation of  $M_2C$  carbides during tempering is very fine with an average size of  $9.6 \times 1.2$  nm measured on 130 carbides (see Fig. 13) and seems to be homogeneously



distributed within the matrix, as already shown by APT. The shape of the  $M_2C$  particles is very elongated with an aspect ratio near 10. The main conclusion can be summarized as follows: the 1060 °C austenitizing temperature contributes to a fine and dispersed precipitation of  $M_2C$  carbides after tempering, thanks to a high supersaturation as well as a homogeneous distribution of carbide-forming elements.

The average chemical composition of the  $M_2C$  carbides measured by atom probe is Mo-rich with a significant content of Cr, W and V (see Fig. 14).

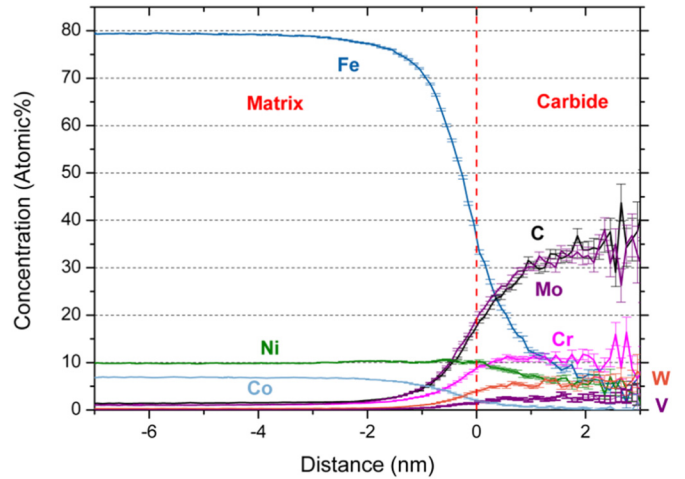


**Fig. 14.** Proximity histogram of the 98 interfaces precipitate/matrix.

The chemical composition of  $M_2C$  measured by atom probe is in quite good agreement with the ThermoCalc® calculations (see Fig. 15). The  $M_2C$  carbides contain mainly Mo and Cr with approx. 10% W and a small amount of Fe and V, as shown in Fig. 15 and Table 5.

However, the chemical composition of the carbides in M54® is quite different from the composition measured in AerMet® 100 and AF1410 steels (see Table 5). Indeed, the main difference comes from the W content in  $M_2C$  carbides for the M54® steel. W has a slower diffusivity than other carbide-forming elements and stabilizes  $M_2C$  carbides for long duration tempering [49] which guarantee the mechanical properties in a wide range of tempering condition.

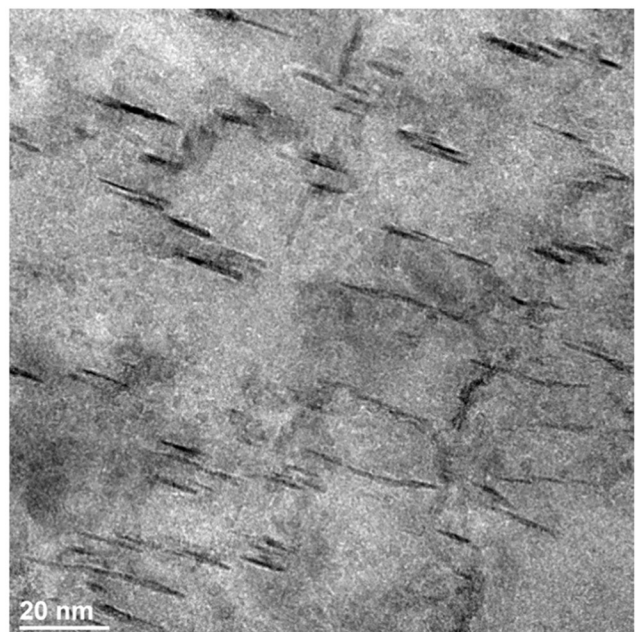


**Fig. 13.** Bright-field TEM images of thin foils of tempered sample at 516 °C for 10 h.

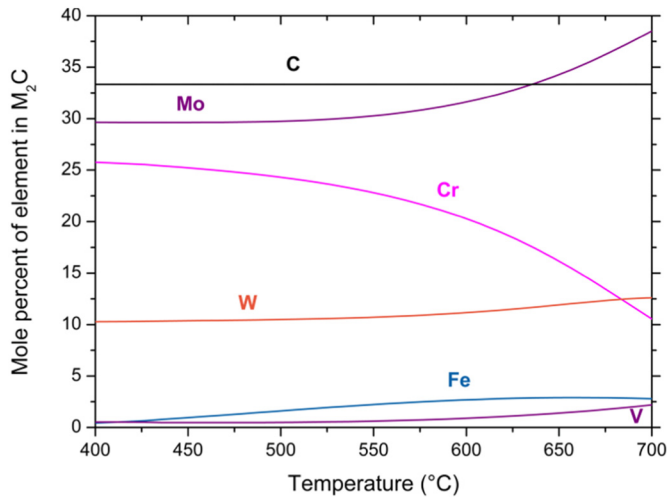


Fig. 15. Chemical composition of M<sub>2</sub>C in M54<sup>®</sup> calculated with TCF3 ThermoCalc<sup>®</sup> database.

Table 5

Comparison of carbide composition of different UHS steels hardened by M<sub>2</sub>C carbide precipitation according to ThermoCalc<sup>®</sup> calculations and experimental measurements.

Steel (Tempering)	AF1410 (510 °C)	AerMet <sup>®</sup> 100 (482 °C)	M54 <sup>®</sup> (516 °C)
Calculated ThermoCalc <sup>®</sup> composition	(Cr <sub>0.63</sub> Mo <sub>0.37</sub> ) <sub>2</sub> C	(Cr <sub>0.71</sub> Mo <sub>0.29</sub> ) <sub>2</sub> C	(Mo <sub>0.45</sub> Cr <sub>0.36</sub> W <sub>0.155</sub> Fe <sub>0.027</sub> V <sub>0.008</sub> ) <sub>2</sub> C
Experimental composition	(Cr <sub>0.686</sub> Mo <sub>0.278</sub> Fe <sub>0.036</sub> ) <sub>2</sub> C [50]	(Cr <sub>0.75</sub> Mo <sub>0.125</sub> Fe <sub>0.125</sub> ) <sub>2</sub> C [15]	(Mo <sub>0.5</sub> Cr <sub>0.125</sub> W <sub>0.1</sub> Fe <sub>0.1</sub> Ni <sub>0.1</sub> V <sub>0.025</sub> ) <sub>2</sub> C

Moreover, very few cementite precipitates are observed in the M54<sup>®</sup> steels. This fact also contributes to the high fracture toughness value measured after tempering. Indeed, cementite is well known to strongly reduce the fracture toughness of high strength steels [34], particularly if the iron carbide is located at the interlath site. The W in M<sub>2</sub>C carbides allows a long duration of the tempering treatment resulting in the total dissolution of cementite without coarsening of M<sub>2</sub>C carbides.

#### 4. Conclusion

Ferrium<sup>®</sup> M54<sup>®</sup> steel was developed by QuesTek using intensive thermodynamic calculations [51]. An excellent strength/fracture toughness balance is achieved with a UTS reaching 1965 MPa and a K<sub>1C</sub> values up to 110 MPa√m. The main goal of this work is to provide experimental evidence and arguments explaining the outstanding UTS/K<sub>1C</sub> balance of properties the work is focused on the precipitation identification during the heat treatment by a different scale microstructural study using advanced experimental tools (XRD, TEM, APT). To this end, the optimization of austenitizing conditions is of primary importance, in conjunction with the solutionizing of alloying elements needed for precipitation during tempering. The main results can be summarized as follows:

- Microstructure in the as-quenched state (after cryogenic treatment) can be defined as a Ti-rich MC carbide precipitation with a size from 50 nm to 120 nm in a martensitic matrix which is highly supersaturated in carbide-forming elements. In addition, those elements are homogeneously distributed within the matrix, according to length-diffusion calculations.
- The addition of small amount of titanium has led to full dissolution of the Mo- and W-rich carbides. Types of precipitates which control the grain size during the austenitization and which strengthen the

steel during the tempering are then totally different.

- This final microstructure is obtained thanks to the proper solutionizing of alloying elements during austenitizing at high temperature (1060 °C) which results in:
  - A high supersaturation before tempering.
  - A homogeneously distributed nucleation of carbides.
- Microstructure in the tempered state 516 °C/10 h is characterized by a homogeneously distributed precipitation of nanometer-sized M<sub>2</sub>C carbides. These carbides contain W, which reduces their coarsening rate.

#### Acknowledgements

Atom-probe tomography was performed at the Northwestern University Center for Atom-Probe Tomography (NUCAPT). The LEAP tomograph at NUCAPT was purchased and upgraded with grants from the NSF-MRI (DMR-0420532) and ONR-DURIP (N00014-0400798, N00014-0610539, N00014-0910781, N00014-1712870) programs. NUCAPT received support from the MRSEC program (NSF DMR-1121262) at the Materials Research Center, the SHyNE Resource (NSF ECCS-1542205), and the Initiative for Sustainability and Energy (ISEN)

at Northwestern University. Special thanks to Dr. Dieter Isheim for his analyses and invaluable help.

Assistance provided by QuesTek Innovations LLC through Chris Kern and Ricardo K. Komai.

#### Data availability

The raw/processed data required to reproduce these findings cannot be shared at this time as the data also forms part of an ongoing study.

#### References

- [1] H.M. Flower, High Performance Materials in Aerospace, Springer Netherlands, Dordrecht, 1995, <http://dx.doi.org/10.1007/978-94-011-0685-6>.
- [2] A.K. Kundu, Aircraft Design, Cambridge University Press, Cambridge, 2010, <http://dx.doi.org/10.1017/CBO9780511844652>.
- [3] G.B. Olson, Computational design of hierarchically structured materials, Science 277 (1997) 1237–1242, <http://dx.doi.org/10.1126/science.277.5330.1237> (80-).
- [4] H. Jou, Lower-Cost, Ultra-High-Strength, High-Toughness Steel, US Patent 2010/0230015 A1, (2010).
- [5] W.M. Garrison, Ultrahigh-strength steels for aerospace applications, JOM 42 (1990) 20–24, <http://dx.doi.org/10.1007/BF03220942>.
- [6] D.S. Dabkowski, P.J. Konkol, L.F. Porter, A.M. Rathbone, Nickel, Cobalt, Chromium Steel, US Patent 3,502,462A, (1970).
- [7] C.D. Little, P.M. Machmeier, High Strength Fracture Resistant Weldable Steels, US Patent 4,076,525, (1978).
- [8] G. Haidemenopoulos, Dispersed-Phase Transformation Toughening in Ultra-High-Strength Steels (PhD Thesis), Massachusetts Institute of Technology, 1988.
- [9] K.J. Handerhan, W.M. Garrison, N.R. Moody, A comparison of the fracture behavior of two heats of the secondary hardening steel AF1410, Metall. Trans. A. 20 (1989) 105–123, <http://dx.doi.org/10.1007/BF02647498>.
- [10] K.J. Handerhan, W.M. Garrison, Effects of rare earth additions on the mechanical properties of the secondary hardening steel AF1410, Scr. Metall. 22 (1988) 409–412, [http://dx.doi.org/10.1016/S0036-9748\(88\)80215-1](http://dx.doi.org/10.1016/S0036-9748(88)80215-1).
- [11] W.M. Garrison, J.L. Maloney, Lanthanum additions and the toughness of ultra-high strength steels and the determination of appropriate lanthanum additions, Mater. Sci. Eng. A 403 (2005) 299–310, <http://dx.doi.org/10.1016/j.msea.2005.05.021>.

- [12] R.M. Hemphill, D.E. Wert, P.M. Novotny, M.L. Schmidt, High Strength, High Fracture Toughness Alloy, US Patent 5,268,044, (1993).
- [13] C.D. Kantner, Designing Strength, Toughness, and Hydrogen Resistance: Quantum Steel, Northwestern University, 2002 (PhD Thesis).
- [14] C.J. Kuehmann, G.B. Olson, H. Jou, Nanocarbide Precipitation Strengthened Ultrahigh-Strength, Corrosion Resistant, Structural Steels, US Patent 7,160,399B2, (2007).
- [15] R. Ayer, P.M. Machmeier, Transmission electron microscopy examination of hardening and toughening phenomena in Aermet 100, Metall. Trans. A. 24 (1993) 1943–1955, <http://dx.doi.org/10.1007/BF02666329>.
- [16] G.B. Olson, T.J. Kinkus, J.S. Montgomery, APFIM study of multicomponent M2C carbide precipitation in AF1410 steel, Surf. Sci. 246 (1991) 238–245, [http://dx.doi.org/10.1016/0039-6028\(91\)90421-N](http://dx.doi.org/10.1016/0039-6028(91)90421-N).
- [17] P.M. Machmeier, C.D. Little, M.H. Horowitz, R.P. Oates, Development of a strong (1650MNm<sup>-2</sup> tensile strength) martensitic steel having good fracture toughness, Met. Technol. 6 (1979) 291–296, <http://dx.doi.org/10.1179/030716979803276138>.
- [18] C. Wang, C. Zhang, Z. Yang, Austenite layer and precipitation in high Co–Ni maraging steel, Micron 67 (2014) 112–116, <http://dx.doi.org/10.1016/j.micron.2014.07.008>.
- [19] C. Wang, C. Zhang, Z. Yang, J. Su, Y. Weng, Analysis of fracture toughness in high Co–Ni secondary hardening steel using FEM, Mater. Sci. Eng. A 646 (2015) 1–7, <http://dx.doi.org/10.1016/j.msea.2015.08.003>.
- [20] E.U. Lee, M. Stanley, B. Pregger, C. Lei, E. Lipnickas, Ferrium M54 Steel, Patuxent River, Maryland, (2015).
- [21] G.L. Pioszak, PhD Thesis, Hydrogen Assisted Cracking of Ultra-High Strength Steels, University of Virginia, 2015.
- [22] M. Schmidt, M.J. Gore, Solution treatment effects in AF1410 steel, Innov. Ultrah. Strength Steel Technol. 34th Sagamore Army Mater. Res. Conf, 1987, pp. 407–424.
- [23] K.K. Sankaran, R.S. Mishra, Metallurgy and Design of Alloys with Hierarchical Microstructures, Elsevier Science Publishing Co Inc, 2017.
- [24] P. Michaud, D. Delagnes, P. Lamesle, M.H. Mathon, C. Levaillant, The effect of the addition of alloying elements on carbide precipitation and mechanical properties in 5% chromium martensitic steels, Acta Mater. 55 (2007) 4877–4889, <http://dx.doi.org/10.1016/j.actamat.2007.05.004>.
- [25] G.B. Olson, Overview: Science of Steel, Innov. Ultrah. Strength Steel Technol. 34th Sagamore Army Mater. Res. Conf, 1987, pp. 3–66.
- [26] M.J. Gore, G.B. Olson, M. Cohen, Grain-refining dispersions and properties in ultrahigh-strength steels, Innov. Ultrah. Strength Steel Technol. 34th Sagamore Army Mater. Res. Conf, 1987, pp. 425–442.
- [27] QuesTek, Processing Information QPI-M54, (2012).
- [28] K.E. Burke, Chemical extraction of refractory inclusions from iron- and nickel-base alloys, Metallography 8 (1975) 473–488, [http://dx.doi.org/10.1016/0026-0800\(75\)90023-3](http://dx.doi.org/10.1016/0026-0800(75)90023-3).
- [29] E. Cabrol, C. Bellot, P. Lamesle, D. Delagnes, E. Povoden-Karadeniz, Experimental investigation and thermodynamic modeling of molybdenum and vanadium-containing carbide hardened iron-based alloys, J. Alloys Compd. 556 (2013) 203–209, <http://dx.doi.org/10.1016/j.jallcom.2012.12.119>.
- [30] B.W. Krakauer, D.N. Seidman, Systematic procedures for atom-probe field-ion microscopy studies of grain boundary segregation, Rev. Sci. Instrum. 63 (1992) 4071–4079, <http://dx.doi.org/10.1063/1.1143214>.
- [31] B.W. Krakauer, J.G. Hu, S.-M. Kuo, R.L. Mallick, A. Seki, D.N. Seidman, J.P. Baker, R.J. Loyd, A system for systematically preparing atom-probe field-ion-microscope specimens for the study of internal interfaces, Rev. Sci. Instrum. 61 (1990) 3390–3398, <http://dx.doi.org/10.1063/1.1141590>.
- [32] J.H. Bunton, J.D. Olson, D.R. Lenz, T.F. Kelly, Advances in pulsed-laser atom probe: instrument and specimen design for optimum performance, Microsc. Microanal. 13 (2007) 418–427, <http://dx.doi.org/10.1017/S1431927607070869>.
- [33] B. Sundman, B. Jansson, J.-O. Andersson, The Thermo-Calc databank system, Calphad 9 (1985) 153–190, [http://dx.doi.org/10.1016/0364-5916\(85\)90021-5](http://dx.doi.org/10.1016/0364-5916(85)90021-5).
- [34] G.R. Speich, D.S. Dabkowski, L.F. Porter, Strength and toughness of Fe-10Ni alloys containing C, Cr, Mo, and Co, Metall. Trans. 4 (1973) 303–315, <http://dx.doi.org/10.1007/BF02649630>.
- [35] C.J. Kuehmann, Thermal Processing Optimization of Nickel-Cobalt Ultrahigh-Strength Steels, Northwestern University, 1994 (PhD Thesis).
- [36] M.A. Rhoads, E.L. Raymond, W.M. Garrison, High strength, high fatigue structural steel, US Patent 5,393,488, 1995.
- [37] R.W.K. Honeycombe, Steels microstructure and properties, Metallurgy (1981).
- [38] G.R. Speich, W.C. Leslie, Tempering of steel, Metall. Trans. 3 (1972) 1043–1054, <http://dx.doi.org/10.1007/BF02642436>.
- [39] D. Delagnes, F. Pettinari-Sturmel, M.H. Mathon, R. Danoix, F. Danoix, C. Bellot, P. Lamesle, a. Grellier, Cementite-free martensitic steels: a new route to develop high strength/high toughness grades by modifying the conventional precipitation sequence during tempering, Acta Mater. 60 (2012) 5877–5888, <http://dx.doi.org/10.1016/j.actamat.2012.07.030>.
- [40] K. Sato, Improving the Toughness of Ultrahigh Strength Steel, University of California, Berkeley, 2002 (PhD Thesis).
- [41] J. Naylor, R. Blondeau, The respective roles of the packet size and the lath width on toughness, Metall. Trans. A. 7 (1976) 891–894, <http://dx.doi.org/10.1007/BF02644090>.
- [42] B. Białobrzęska, Ł. Konat, R. Jasiński, The influence of austenite grain size on the mechanical properties of low-alloy steel with boron, Metals (Basel) 7 (2017) 26, <http://dx.doi.org/10.3390/met7010026>.
- [43] H.E. Lippard, PhD Thesis, Microanalytical Investigations of Transformation Toughened Co-Ni Steels, Northwestern University, 1999.
- [44] J. Daigne, M. Guttman, J.P. Naylor, The influence of lath boundaries and carbide distribution on the yield strength of 0.4% C tempered martensitic steels, Mater. Sci. Eng. 56 (1982) 1–10, [http://dx.doi.org/10.1016/0025-5416\(82\)90176-8](http://dx.doi.org/10.1016/0025-5416(82)90176-8).
- [45] P. Bate, The effect of deformation on grain growth in Zener pinned systems, Acta Mater. 49 (2001) 1453–1461, [http://dx.doi.org/10.1016/S1359-6454\(01\)00033-7](http://dx.doi.org/10.1016/S1359-6454(01)00033-7).
- [46] P.J. Alberry, C.W. Haworth, Interdiffusion of Cr, Mo, and W in Iron, Met. Sci. 8 (1974) 407–412, <http://dx.doi.org/10.1179/msc.1974.8.1.407>.
- [47] R. Ayer, P. Machmeier, On the characteristics of M2C carbides in the peak hardening regime of AerMet 100 steel, Metall. Mater. Trans. A. 29 (1998) 903–905, <http://dx.doi.org/10.1007/s11661-998-0280-1>.
- [48] R. Ayer, P.M. Machmeier, Microstructural basis for the effect of chromium on the strength and toughness of AF1410-based high performance steels, Metall. Mater. Trans. A. 27 (1996) 2510–2517, <http://dx.doi.org/10.1007/BF02652345>.
- [49] H.M. Lee, S.M. Allen, M. Grujicic, Stability and coarsening resistance of M2C carbides in secondary hardening steels, 34th Sagamore Army Mater. Res. Conf, 1987, pp. 127–146.
- [50] H.M. Lee, A.J. Garratt-Reed, S.M. Allen, Composition of M2C phase in tempering of high Co-Ni steels, Scr. Metall. Mater. 25 (1991) 685–688, [http://dx.doi.org/10.1016/0956-716X\(91\)90115-H](http://dx.doi.org/10.1016/0956-716X(91)90115-H).
- [51] G.B. Olson, C.J. Kuehmann, Materials genomics: from CALPHAD to flight, Scr. Mater. 70 (2014) 25–30, <http://dx.doi.org/10.1016/j.scriptamat.2013.08.032>.